



Atlantic Ecosystems Assessment, Forecasting & Sustainability

# Deliverable number 6.2 - Dataset of ocean reanalysis and hindcast simulation version 2

Dissemination level: Public

Related Work Package	WP6 Advances in model predictability
Related task(s)	Task 6.1
Lead beneficiary	Fondazione Centro Euro-Mediterraneo sui Cambiamenti Climatici, CMCC
Author(s)	P.G. Fogli, D. Iovino, S. Masina (CMCC)
Due date	31.08.2023
Submission date	07.09.2023
Type	Report
Status and version	Final, v1.0

**Declaration:** Any work or result described therein is a genuine output of the AtlantECO project. Any other source will be properly referenced where and when relevant.





Table of Content

1	Version History	3
2	Executive summary	4
3	Introduction	5
4	Model configuration and experimental design	6
5	Dataset evaluation	7
5.1	Temperature and salinity	7
5.2	Kinetic energy	8
5.3	Atlantic meridional overturning circulation	10
5.4	The Benguela region	11
6	Data availability	15
7	Conclusion	18
8	Table of figures	19
9	References	19



## 1 Version History

---

Version	Contributor	Summary of changes	Date
0.1	P.G. Fogli	Initial draft	17/08/2023
0.2	D. Iovino, S. Masina	Internal review	28/08/2023
0.3	E. van Sebille	WP leader Review	30/08/2023
0.4	P.G. Fogli	Revision	31/08/2023
0.5	S. Pesant	Coordination review	06/09/2023
0.6	P.G. Fogli	Final revisions	07/09/2023
1.0	E. Trabut	Formatting and submission	07/09/2023



## 2 Executive summary

---

The Deliverable “Dataset of ocean reanalysis and hindcast simulation version 2” is produced as part of the Work Package 6 “Advances in model predictability”. It documents the update of the dataset described in the Deliverable 6.1 “Dataset of ocean reanalysis and hindcast simulation version 1” ([lovino et al., 2022](#)) (hereafter D6.1), realised by extending the multi-year ocean-sea ice simulation from which it is derived to all of 2022. This updated dataset now provides 3D daily mean fields at 1/16° horizontal resolution and in the upper 540m for the whole Atlantic Ocean, that includes the data for the Benguela region, over the entire period from 2009 to 2022.

One variable for one time record is stored per file in CF-compliant NetCDF4 (with lossless compression) for a total size of 17 Tb. The dataset is available, under license [CC BY 4.0](#), upon registration through the CMCC Data Delivery System (DDS) at <https://dds.cmcc.it/#/dataset/glob16-atlantic-ocean> and it is identified by the following digital object identifier doi: [10.25424/cmcc-x754-gh24](https://doi.org/10.25424/cmcc-x754-gh24).

*This document is based on the terms and conditions established in the Grant Agreement (GA) and its Annexes, as well as in the Consortium Agreement (CA).*



### 3 Introduction

---

The multi-year validated ocean-sea ice simulation at  $1/16^\circ$  results was described in the deliverable D6.1 ([lovino et al., 2022](#)) as Version 1 of the CMCC dataset, covering the integration period 1958-2018. Since the delivery of D6.1, several publications based on the same experiment have been released or are currently under review. In particular, a detailed validation of the CMCC global eddy ocean model is presented in the reference publication by [lovino et al. \(2023\)](#), that also explores the benefit of an eddy-rich resolution modelling framework versus eddy-permitting and non-eddy systems. The impacts of the resolved mesoscale eddies on the mixed layer depth (MLD) ([Treguier et al., 2023](#)) and the role of horizontal resolution on the hydrography and circulation of the Arctic Ocean ([Wang et al. 2023](#)) are investigated in a multi-model intercomparison framework.

One of the goals of Work Package 6 is the development of novel methods to compute Lagrangian connectivity of water, nutrients and plankton within and between different regions of the Atlantic Ocean using present-day high-resolution hydrodynamic data. The suitability of the dataset Version 1 for estimating the connectivity pathways and timescales for plankton species with specified constraints on temperature tolerances, by combining Lagrangian modelling with network theory has been demonstrated ([Manral et al., 2023](#)). The update of the dataset in Version 2 offers a longer time series of the same high-frequency 3D tracers and dynamic fields at eddy-resolving resolution that allow for the computation of more reliable statistics and the exploitation of a wider range of dynamic regimes in order to help quantify and reduce uncertainties in physical connectivity between biogeographic regions.



## 4 Model configuration and experimental design

---

The dataset described in this document is obtained by producing another four years of the simulation already presented in D6.1, thus extending the dataset length to the 14-year period from 2009 to 2022. The model configuration and experimental setup (based on the Ocean Model Intercomparison Project (OMIP) protocol by [Griffies et al. \(2016\)](#)) are unchanged. The only modification is related to the atmospheric forcing and continental river discharge which are updated from JRA55-do version 1.4 ([Tsuji no et al., 2018](#)) to the latest release ([Tsuji no et al., 2021](#)). This update was necessary to continue the hindcast simulation from January 2019 onward. JRA55-do version 1.5 also includes two fixes to correct 1) the surface atmospheric fields around the anti-cyclonically rotating tropical cyclones and 2) the surface meteorological variables (specific humidity, air temperature, and wind vector) after 2016.

A detailed description of the model configuration and experimental setup is given in D6.1 ([lovino et al., 2022](#)), together with a validation of the global ocean circulation in the reference publication on the CMCC global eddying ocean model ([lovino et al., 2023](#)).



## 5 Dataset evaluation

---

In this section, we present a set of basic large-scale diagnostics for assessing the relative quality and variability of the eddy-rich ocean simulation that includes the newly produced years. In particular, we focus on the stability of the simulation under the forcing update and on the Benguela Current system, one of the major eastern boundary upwelling systems of the world. The Benguela Current region is situated along the coast of southwestern Africa, stretching from east of the Cape of Good Hope in the south, northwards to Cabinda in Angola and encompassing the full extent of Namibia's marine environment.

We use key metrics common in climate modelling, applied to the global domain, the Atlantic Sector and a zoom on the Benguela upwelling region.

### 5.1 Temperature and salinity

Here we present the temporal evolution of the globally-averaged (potential) temperature and salinity in Version 2 of the dataset. The drifts with respect to the initial conditions of the annual-mean temperature and salinity are represented in [Figure 1](#), where the time series of the volume-averaged fields are shown for the whole column depth and for the upper 500m of the ocean. Relative to the beginning of the simulation, the upper-ocean temperature increase, already seen in D6.1 until 2018, continues with a similar trend to the end of 2022. This is consistent with estimates of the upper-ocean heat content (OHC) from the Institute of Atmospheric Physics (IAP, [Cheng et al., 2017](#)). [lovino et al. \(2023\)](#) show that, after an initial model adjustment, the linear trend of the annual mean OHC is about  $3.096 \times 10^{22}$  J/decade over the first 300m, and closely follows the  $3.033 \times 10^{22}$  J/decade estimated over the period 1970-2018 ([Cheng et al., 2017](#)). The upper-ocean salinity shows the same overall stability and presents only small changes, with a very weak freshening.

The temperature and salinity averaged over all depths present much smaller changes, due to compensation between upper and deeper layers. No change in both trend and interannual variability is evident in recent years. The temporal evolution in each of the major ocean basins (not shown) mimics that of the global domain.

In Version 2 of the dataset, global and regional biases, as well as simulated variability from seasonal to interannual time scales, do not show any relevant change with respect to previous analysis ([lovino et al., 2022](#) and [2023](#)), thus are not shown.

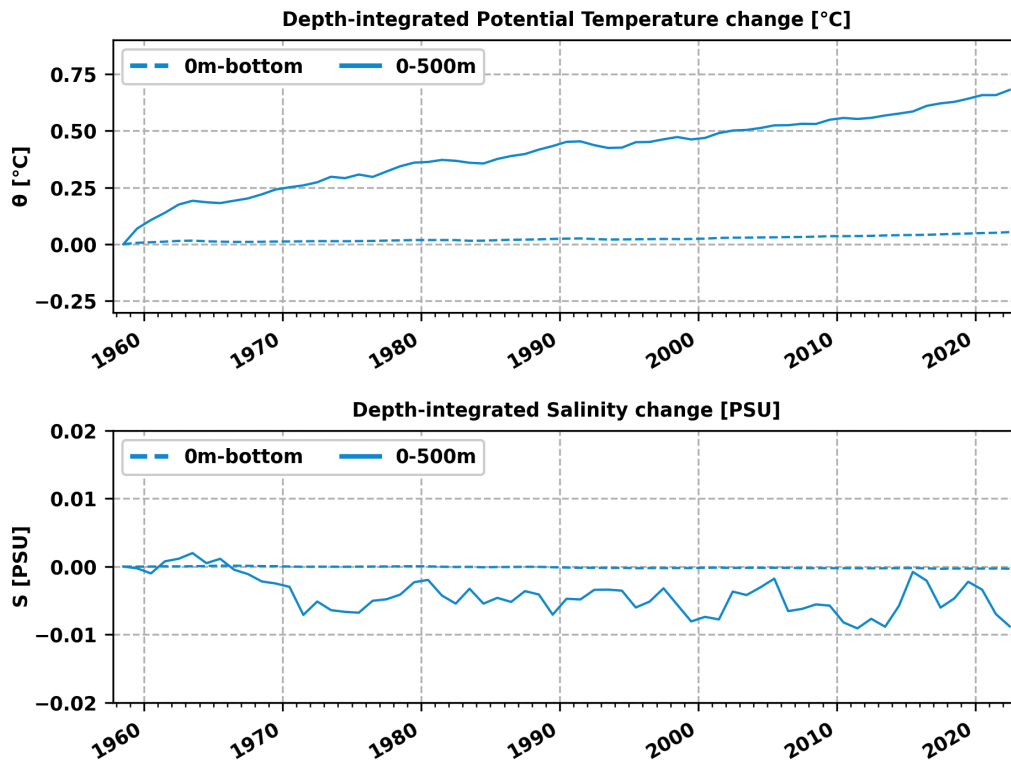


**Figure 1:** Time evolution of global temperature (°C) and salinity (psu) change (relative to initial conditions) vertically averaged in the upper 500m (solid lines) and on the full depth (dashed lines).

## 5.2 Kinetic energy

The time evolution of the domain-averaged kinetic energy of the system is illustrated in [Figure 2](#), where the time series of the total specific kinetic energy (KE) [defined as  $\frac{1}{2} \cdot (u^2 + v^2)$ , where  $u$  and  $v$  are the monthly averages of the horizontal velocity components] and its eddy component (EKE) [defined as  $\frac{1}{2} \cdot (u'^2 + v'^2)$ , where  $u'$  and  $v'$  are the respective deviations] are shown. After a quick spin-up during the first years of the simulation, a stable equilibrium of the kinetic energy is established in two to three decades, illustrating the extent to which a quasi-steady state has been reached by the end of the simulation. As pointed out in previous analysis, the kinetic energy remains significantly lower than what can be inferred from observations and even higher-resolution models ([Chassignet and Xu, 2017](#)).

The eddy kinetic energy (EKE) component accounts for ~65% of the total basin-averaged budget ([Iovino et al., 2023](#)), indicating that most of the energy comes from the eddy field.

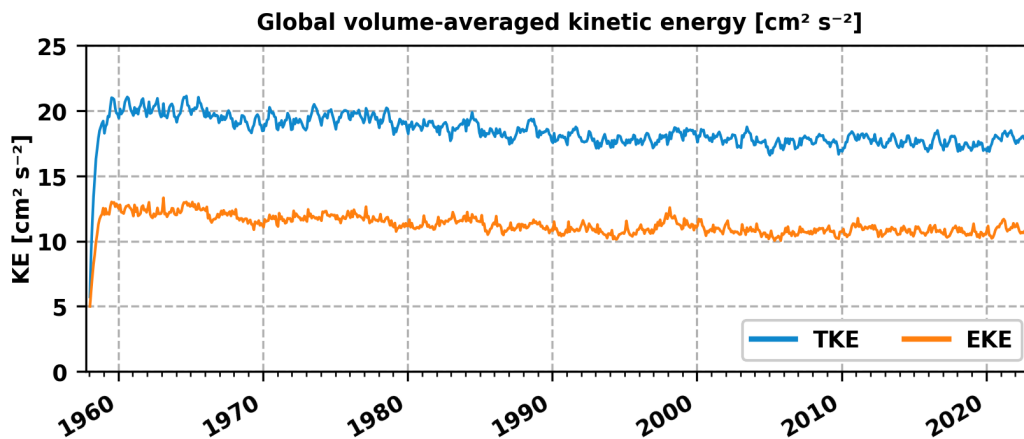


**Figure 2:** Time evolution of the global volume-averaged total (TKE) and eddy (EKE) specific kinetic energy ( $\text{cm}^2/\text{s}^2$ ) from monthly-mean fields.

[Figure 3](#) shows the temporal evolution of eddy kinetic energy (EKE) for the Atlantic Ocean at 15m and 250m, and its decomposition between the Northern and Southern components. In the top layer, the basin-wide eddy kinetic energy is dominated by the North Atlantic contribution with a well-defined seasonal cycle that is absent in the Southern basin. Overall, the Atlantic EKE increases roughly by 30% from the winter minima to the highest values during summer/autumn. The North Atlantic EKE seems to present a lower mean value and a reduced seasonal cycle during the first years of the analysed period. This is not reproduced in the Southern Ocean, which overall shows a lower variability. The EKE computed at 250m depth is comparable in the two hemispheres with the Southern Ocean that tends to dominate the basin-scale seasonal and interannual variability. At both depths, there is no evidence of abrupt changes in the time variability during the newly simulated years, demonstrating the low impacts of the updated forcing. There are no significant changes in the global and regional patterns of total and eddy kinetic energy either, when the extra years are added (not shown) with respect to previous analysis up to 2018 ([lovino et al., 2022](#))

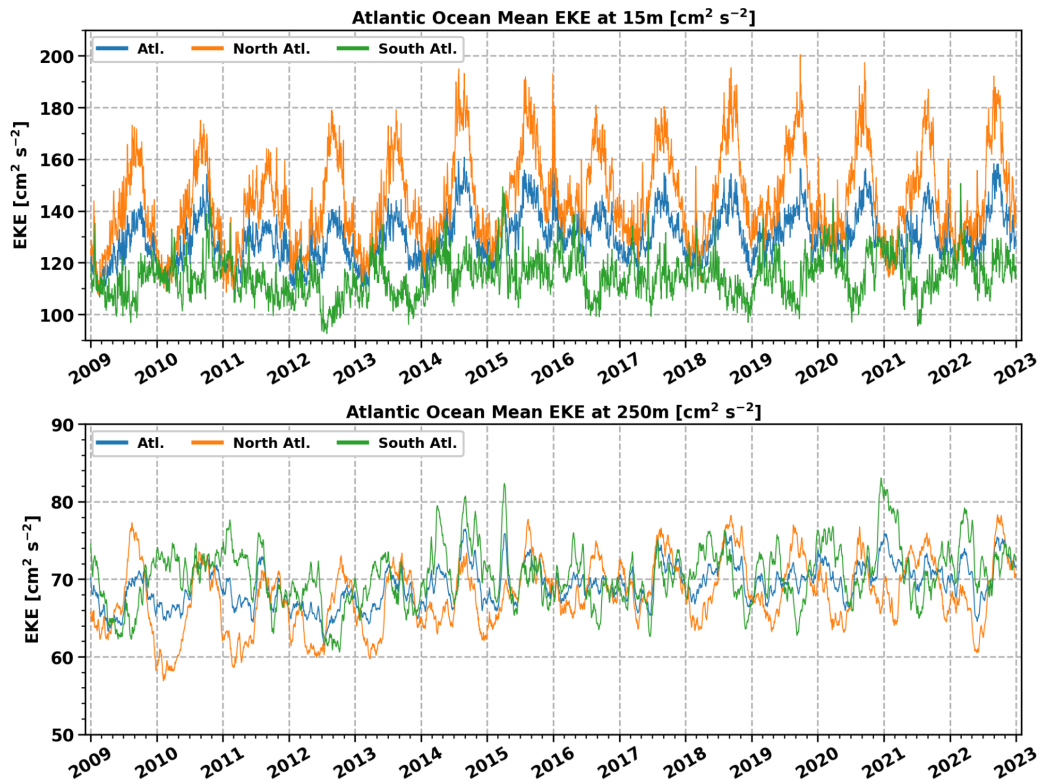


**Figure 3:** Time evolution of the 15m (top panel) and 250m (bottom panel) Atlantic-averaged specific eddy kinetic energy ( $\text{cm}^2/\text{s}^2$ ) for the years 2009-2022, computed from daily-mean velocity fields.

### 5.3 Atlantic meridional overturning circulation

The mean structure and temporal variability of the meridional overturning circulation (MOC) are frequently used to evaluate ocean models performance, being one of the main drivers of climate variability. The time-varying intensity of the Atlantic meridional overturning circulation (AMOC) has been measured across fixed sections at several latitudes, for instance at  $26.5^\circ\text{N}$  (since spring 2004) and  $34.5^\circ\text{S}$  (since 2009).

We compare the time series of the strength of the AMOC at  $26.5^\circ\text{N}$  from the GLOB16 integration and the estimates made available by the RAPID-MOCHA-WBTS program (Moat et al., 2021) in Figure 4a. In the RAPID estimate, the magnitude of the AMOC is defined as the maximum of the stream function in depth space and represents the total northward transport above the overturning depth. Compared to the mean observed value of  $16.9 \pm 3.44$  Sv for the period 2004-2020, the modelled AMOC transport is weaker reaching a mean value of 13.7 Sv (other OMIP2 high-resolution simulations range from 14 to 20 Sv in Chassignet et al., 2020). As in other OMIP simulations, the AMOC in GLOB16 decreases during the first decade, toward a steady state with no apparent trend thereafter. The modelled time evolution is in good agreement with the RAPID interannual variability, following it closely particularly in the last 12 years of the observation. Weak AMOC events observed in 2010, 2011, 2013 and 2018 are well captured. Much of the variability at this latitude on interannual timescales is dominated by wind forcing (Pillar et al., 2016), contrary the previous hypothesis that AMOC variations are driven by the buoyancy forcing in subpolar regions (Kuhlbrodt et al., 2007). The newly produced years of the simulation provided in Version 2 of the dataset are in good agreement also with the observations available from 2019 onward.

The AMOC transport in the Southern Atlantic, shown in Figure 4b, is estimated on direct daily measurements at  $34^\circ\text{S}$  from the South Atlantic MOC Basin-wide Array (SAMBA, Meinen et al., 2018), which has a pilot array in 2009-2010 and a second record from 2013 to 2017. It is worth noting that the SAMBA calculation method uses a time-mean reference velocity, so the observations at  $34^\circ\text{S}$  provide the variability of the AMOC at the same

latitude rather than an observational mean. The observations yield a peak-to-peak range of 54.6 Sv on daily means (not shown) and in excess of 20 Sv on monthly means. The AMOC has a time mean meridional transport over the full 2009–2017 period (considering the ~3-year gap) of  $14.7 \pm 8.3$  Sv. Over the same period, the time mean AMOC transport in GLOB16 is 12.1 Sv, with a reduced interannual variability.

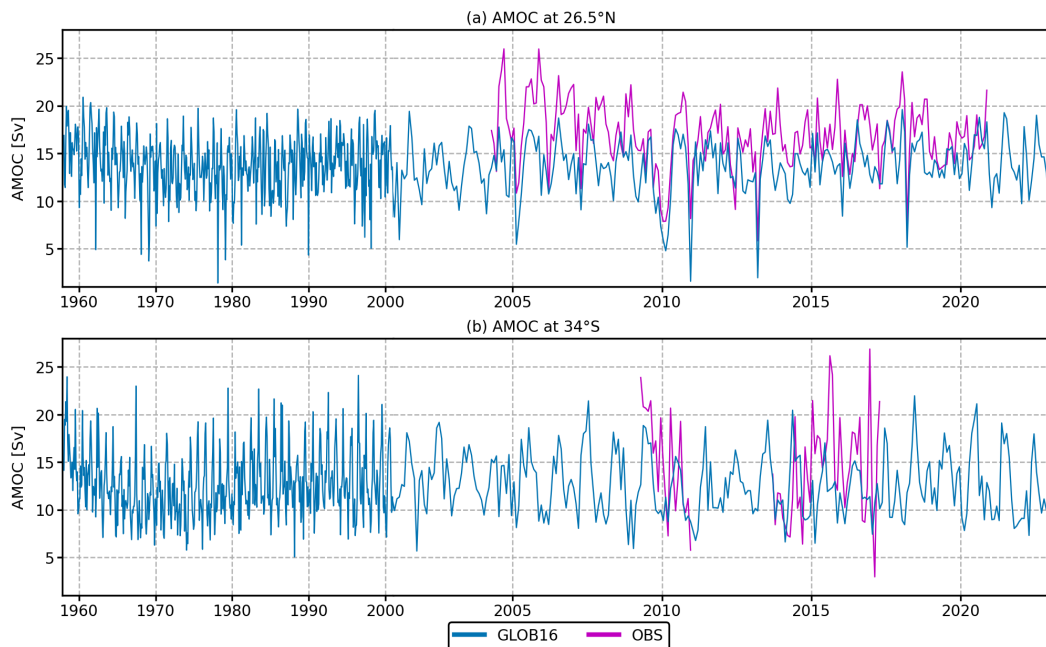


**Figure 4:** Time evolution of monthly mean AMOC transports, defined as the maximum value of the Atlantic overturning streamfunction (blue line) computed (a) across 26.5°N and compared to RAPID estimates, and (b) 34°S compared to SAMB'A record. Horizontal scale is compressed prior to the year 2000.

## 5.4 The Benguela region

The Benguela system is one of the major eastern boundary upwelling systems of the world. The Benguela Current is the eastern limb of the South Atlantic sub-tropical gyre and also encompasses the Benguela Upwelling System (BUS), which spans along the southwestern coast of Africa covering the western South African and Namibian coastline roughly from Cape Agulhas (~34°S) to the Angola Benguela Frontal Zone. The northern boundary of the upwelling system is coincident with the Angola Benguela Frontal Zone where the warm Angola Current meets the cool Benguela upwelling regime, and the southern boundary is influenced by the thoroughfare of Agulhas rings that form at the retroflexion. The South Easterly trade winds along south-west African coasts provide the driving force for the Benguela Current which feeds water masses into the South Equatorial Current as part of the basin-scale wind-driven oceanic circulation. Inshore of the Benguela Current proper, the south easterly winds cause coastal upwelling. The principal upwelling centre is situated offshore the Lüderitz area in southern Namibia. A schematic overview of the ocean circulation in the region is shown in [Figure 5](#).

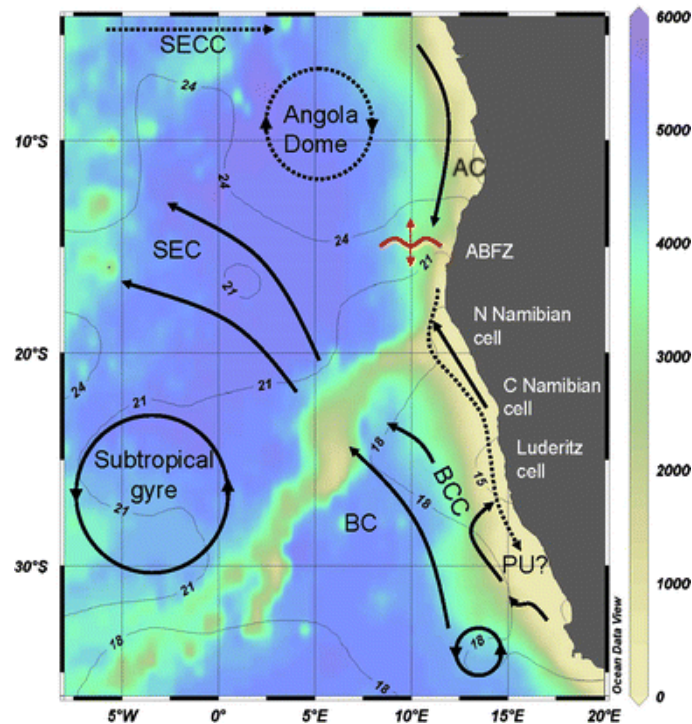


**Figure 5.** Schematic overview of the ocean features in the Benguela region (from [Emeis et al., 2009](#)). Bathymetry of the South East Atlantic (shaded colours) with climatological sea surface temperatures (contour lines in °C, from [Gouretski and Koltermann, 2004](#)). Surface currents are represented by solid lines and subsurface currents by dashed lines. AC Angola Current, ABFZ Angola-Benguela frontal zone, BC Benguela Ocean current, BCC Benguela coastal current, PU poleward undercurrent, SEC south equatorial current, SECC south equatorial counter current.

[Figure 6](#) shows the near-surface ocean circulation simulated by GLOB16 compared with the Ocean Surface Current Analyses Real-time (OSCAR; [https://podaac.jpl.nasa.gov/dataset/OSCAR\\_L4\\_OC\\_FINAL\\_V2.0](https://podaac.jpl.nasa.gov/dataset/OSCAR_L4_OC_FINAL_V2.0); [ESR, 2022](#)) dataset in the Benguela domain. The ocean speed fields are vertically averaged over a surface layer thickness of 30 m for the 2009-2022 period, using daily output. The OSCAR field is calculated from satellite datasets and consists of a geostrophic term, a wind-driven term, and a thermal wind adjustment, interpolated on a 0.25° grid.

The large-scale current system represented by GLOB16 qualitatively compares very well with observations. The model captures the major current systems of this Southern Atlantic sector reproducing each of the local maxima and minima in OSCAR, but it tends to underestimate the magnitude of observed surface velocity in particular in the Angola gyre between 10°S - 25°S.

The observed and simulated current systems show the Benguela Current originates in the south from the South Atlantic Current and the Agulhas current flowing around the southern tip of Africa and reversing to the east in the Agulhas ring. The meridional velocity within the Benguela Current weakens between 35°S and 30°S, as the current moves north westward. In this latitude range, two regimes are detected: in the eastern sector near the African coast, the circulation is characterised by relatively strong northward flow, while in the western sector, it has relatively weak alternating flow with several distinct recirculation features in the mean field. At ~30°S, the current splits into the main Benguela current heading northwest, and the Benguela Coastal Current, which flows as a slow current along the continental margin. These currents are driven by the predominantly southerly and southeasterly winds (e.g. [Shannon, 1985](#)). Off the coast of South Africa and Namibia, these winds drive coastal upwelling of cold, nutrient-rich South Atlantic Central Water.

The northern boundary of the Benguela current system is formed by the Angola-Benguela Front zone where the zonal velocity component dominates. This frontal zone fluctuates north-southward depending on the strength of the Benguela and Angola Currents and associated factors such as wind forcing. It is worth noting the small

intense feature near the coast around 16°S, the latitude where the frontal zone is generally centered, and the cold and nutrient-rich seawater of the Benguela current meet the warm, saline, and nutrient-poor seawater of the Angola current. At its southern boundary, the system is bounded by the extremely dynamic Agulhas Current, which is characterised by eddies and filaments which leak from the retroflexion of the Agulhas Current.

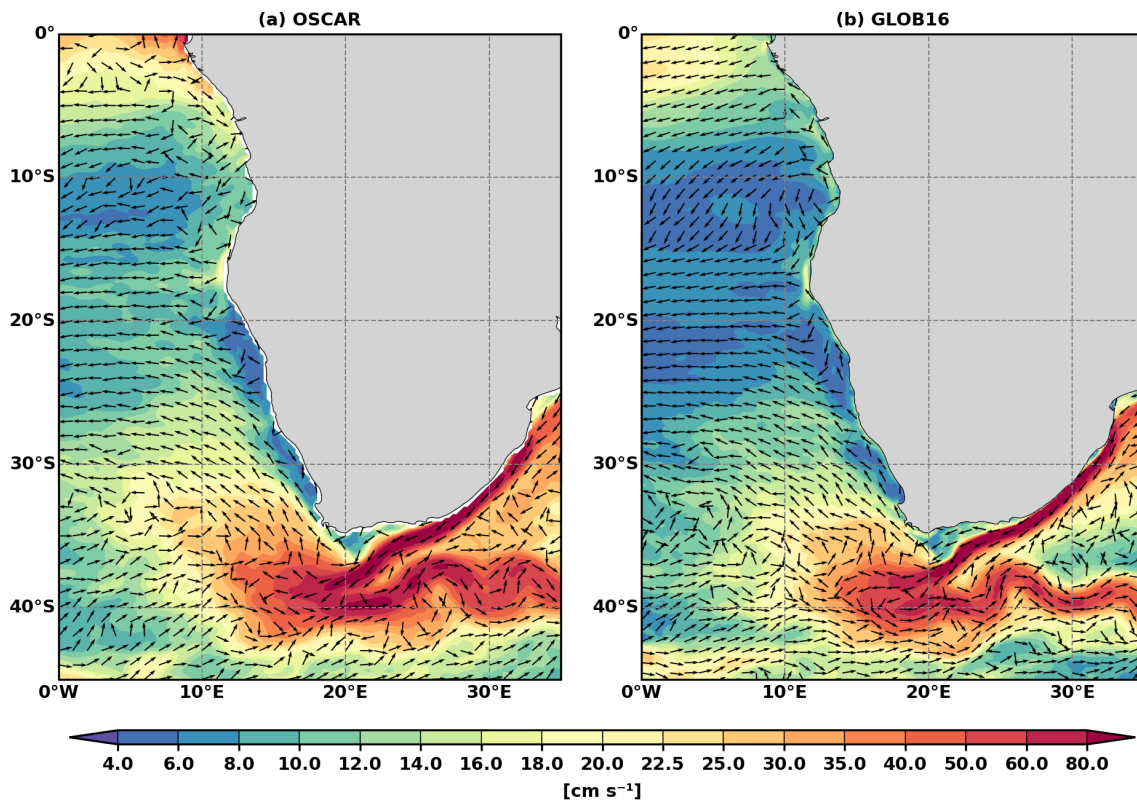


**Figure 6:** Upper-ocean horizontal current (in  $\text{cm s}^{-1}$ ) vertically averaged from 0m to 30m for (a) OSCAR and (b) GLOB16 over the period 2009-2022. Arrows indicate the flow direction, and the shading represents magnitude.

This portion of the west coast of southern Africa is dominated by the strong, wind-driven, coastal upwelling system which results in substantial offshore SST gradients (e.g., [Hutchings et al. 2009](#)). [Figure 7](#) shows the sea surface temperature (SST) in the Benguela region as simulated by GLOB16 as mean over the 2009-2022 period, compared with the ESA SST CCI and C3S global Sea Surface Temperature Reprocessed (<https://doi.org/10.48670/moi-00169>; [Good et al., 2020](#)). The overall SST spatial structure is properly captured by the model. The position and thermal gradient of the frontal zones delimiting the Benguela current are realistically reproduced. The Benguela upwelling area stretches from 37°S to about 14°S in the observed fields; this area is smaller in GLOB16, with the coldest temperature between 35°S and 25°S. The northern Benguela system (north of ~30°S) is limited by the warm ABFZ that is a relatively stable SST feature. The southern Benguela system (south of ~30°S) has a strong seasonality (not shown) with increased upwelling favourable winds in the austral summer months. Among the several upwelling cells along the coast, the Lüderitz cell (at about 27°S) is the most intense and is captured by GLOB16. At the southern boundary of the Benguela upwelling system, the Agulhas Current brings warmer surface water. Having warm water at both ends makes the Benguela region unique when compared with the other major upwelling areas of the world ocean. However, the upwelling region, the band of lower SST along the African coast from Cape Agulhas to Cape Frio, is warmer in the model than in the observations, particularly north of Walvis Bay. This is consistent with many previous studies that show a general difficulty of ocean models in reproducing the observed cold SST off the

coast of southwestern Africa, a region where models of comparable resolution are typically affected by a warm bias ([Chassignet et al., 2020](#)).

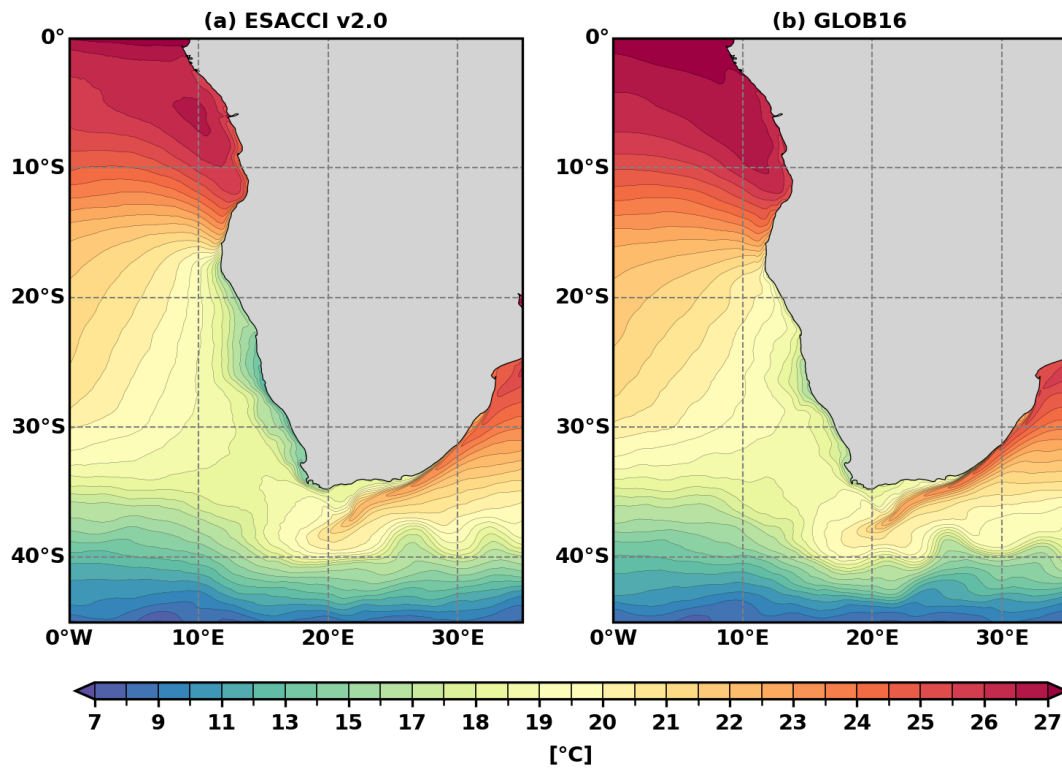


**Figure 7:** Annual mean sea surface temperature (°C) for (a) the ESA CCI SST v2.0 and (b) GLOB16 over the period 2009-2022. Contour interval is 1°C for SST below 17°C, and 0.5°C above.

## 6 Data availability

The updated dataset provided in Task 6.1 consists of daily-mean fields of potential temperature, salinity, horizontal and vertical components of sea water velocity in the upper 540 m of the Atlantic Ocean. The data set covers the last 14 years (2009-2022) of a 65-year hindcast simulation performed with the CMCC ocean-sea ice system at eddying resolution ([lovino et al., 2023](#)) based on the OMIP experimental protocol ([Griffies et al., 2016](#)). The Atlantic region is defined as a rectangular box (1903 x 3896 horizontal grid points and 50 vertical geopotential levels) from 98°W to 21°E and from the Antarctic coastline up to the Nordic Seas (included in the domain). The three-dimensional Benguela region can be arbitrarily cut out of the Atlantic domain.

Model output files are available in the Climate and Forecast (CF)-compliant NetCDF4 binary format (with lossless compression). Each file consists of a CF header containing the relative metadata (variables, dimensions, data type, units, content description, missing value, and global attributes) and the data section that contains the actual values. Each file stores one 3D variable for one time record (daily mean), for a total size of 17 Tb.

The dataset is made available through the CMCC Data Delivery System (DDS, <https://dds.cmcc.it>) that provides a seamless access point for all data produced and used by CMCC through a unified Python Application Program Interface (API). The user can browse the Catalog and the available datasets through the DDS Web Portal, as well as access and download data through the DDS Python API client in a way similar to the C3S Climate Data Store API (<https://cds.climate.copernicus.eu/api-how-to>). Once the dataset of interest is located, the user can select the variable(s), the time interval, the region and the vertical extension (temporal & spatial sub setting) to download and then interactively generate a prototype Python script. A screenshot of the DDS home page is shown in [Figure 8](#) where a subset of the datasets available in the DDS Catalog are visible. The Atlantic Ocean output dataset Version 2 is available, under license [CC BY 4.0](#), at the following URL <https://dds.cmcc.it/#/dataset/glob16-atlantic-ocean>. It is identified by the following digital object identifier doi:[10.25424/cmcc-x754-gh24](https://doi.org/10.25424/cmcc-x754-gh24).

**CMCC DDS**  
Data Delivery System

Home Docs About Contact Us Requests Profile Logout

**ERA5-DOWNSCALED-OVER-ITALY**  
The dataset contains dynamically downscaled ERA5 reanalysis, originally available at  $\approx 31$  km x 31 km horizontal resolution, to 2.2 km x ...

**ERA5-LAND**  
ERA5-Land is a reanalysis dataset providing a consistent view of the evolution of land variables over several decades at an enhanced re...

**ERA5-SINGLE-LEVELS**  
This dataset is related to ERA5 that is the fifth generation ECMWF atmospheric reanalysis of the global climate. Reanalysis combines mo...

**EUROPE-EXTREME-PRECIPITATION-RISK-INDICATORS**  
This dataset provides Climate Impact Indices related to (extreme) precipitation for the European domain. The dataset provides a histori...

**EUROPEAN-CITIES-FLOOD-RISK-INDICATORS**  
The dataset presents climate impact indicators related to extreme precipitation and indicators to evaluate the spatial distribution of ...

**GLOB16-ATLANTIC-OCEAN**  
This dataset provides a set of physical ocean parameters over the Atlantic Ocean region produced using the CMCC GLOB16 eddy-resolving ...

**GLOBAL-SPEI-ENSEMBLE-SIMULATIONS**  
A new Standardized Precipitation Evapotranspiration Index (SPEI) dataset is provided for a reference period 1960-1999 and two future ti...

**MEDSEA-CMIP5-PROJECTIONS-BIOGEOCHEMISTRY**  
The dataset provides a set of biogeochemical parameters over the Mediterranean Sea region which describe the evolution of the system un...

**MEDSEA-RCP45-Sea Surface Temperature anomaly (2090-2099 minus 2000-2009)**  
The dataset provides a set of physical ocean parameters over the Mediterranean Sea region which describe the evolution of the system un...

**Figure 8:** The CMCC Data Delivery System home page (<https://dds.cmcc.it>). Version 2 of the dataset is



visible in the middle-right box.

Registered users can access and download data through the DDS Python API client, available through Anaconda or the Python Package Index (PyPI). The minimum required version is 0.6b1. A brief installation and configuration guide for the DDS API client is available at <https://dds.cmcc.it/#/docs>. A video tutorial and a general presentation of the system are available through the CMCC YouTube channel (<https://www.youtube.com/@CMCCvideo>). An example Python script to download the dataset one daily-mean file at a time is provided in Figure 9 of D6.1. Here we provide in [Figure 9](#) an updated example Python script which shows how to leverage the spatial sub setting capabilities of the DDS to retrieve only the data in a rectangular box over the Benguela Current region in the Southern Atlantic Ocean.



```
import datetime as dt
import ddsapi

# Initialize the client
c = ddsapi.Client()

# Dataset DDS id
dsid = "globl6-atlantic-ocean"

# Query dataset availability
ret = c.datasets(dsid)
if ("detail" in ret):
    raise RuntimeError(ret["detail"])

# Download daily-mean data, 1 day per file at a time
variables = ["thetao", "so", "uo", "vo", "wo"]
years = range(2009, 2023) # 2009-2022
months = range(1, 13) # 1-12
dpm = (31, 29, 31, 30, 31, 30, 31, 31, 30, 31, 30, 31)
#
region="Benguela"
box={"west": 0.0, "east": 21.0, "north": -15.0, "south": -35.0}
#
for var in variables:
    for year in years:
        for month in months:
            for day in range(1, dpm[month]+1):
                #
                # Leap day check
                if (month==2):
                    try:
                        dt.datetime(year=year, month=month, day=day)
                    except:
                        continue
                #
                # retrieve data
                ret = c.retrieve(dsid, "daily",
                    {
                        "variable": [ var, ],
                        "time": {
                            "year": [ str(year), ],
                            "month": [ str(month), ],
                            "day": [ str(day), ]
                        },
                        "area": box,
                        "format": "netcdf"
                    },
                    target="GLOB16_1d_{:s}_{:s}_{:04d}{:02d}{:02d}.nc".format(var,
region, year, month, day))
```

**Figure 9:** Example Python script for the download of the data using the DDS API client showing how to perform spatial subsetting.



## 7 Conclusion

---

The overall goal of this report is to provide an updated description of the ocean dataset produced using the CMCC eddying ocean-sea ice system, GLOB16, forced by JRA55-do for 65 years, based on the Deliverable 6.1, this deliverable includes ocean variables covering the Atlantic basin with additional years from 2019 to 2022. As required by the WP activities, the delivered domain includes the Benguela Current upwelling system as a representative biogeographic region relevant in Lagrangian connectivity studies.

We used a set of large-scale diagnostics for assessing the relative quality and variability of GLOB16 and the consistency of the simulation against the update of the forcing. GLOB16 shows good skill in reproducing the ocean average state and in representing the variability in the upper ocean, on par with other ocean-sea ice models of comparable resolution. No evident drawbacks related to the atmospheric forcing has emerged from the analysis, suggesting that the updated dataset is suitable as a present-day high-resolution hydrodynamic driver for Lagrangian modelling and physical and biogeochemical connectivity studies between biogeographic regions. Moreover, the temporal extension of the dataset provided in Version 2 enables the computation of more reliable statistics and offers a wider range of dynamic regimes to help quantify and reduce uncertainties in connectivity within as well as between biogeographic regions.

## 8 Table of figures

---

**Figure 1:** Time evolution of global temperature ( $^{\circ}\text{C}$ ) and salinity (psu) change (relative to initial conditions) vertically averaged in the upper 500m (solid lines) and on the full depth (dashed lines).

**Figure 2:** Time evolution of the global volume-averaged total (TKE) and eddy (EKE) specific kinetic energy (in  $\text{cm}^2 \text{s}^{-2}$ ) from monthly-mean fields.

**Figure 3:** Time evolution of the 15m (top panel) and 250m (bottom panel) Atlantic-averaged specific eddy kinetic energy (in  $\text{cm}^2 \text{s}^{-2}$ ) for the years 2009-2022, computed from daily-mean velocity fields.

**Figure 4:** Time evolution of monthly mean AMOC transports (in Sv), defined as the maximum value of the Atlantic overturning streamfunction (blue line) computed (a) across  $26.5^{\circ}\text{N}$  and compared to RAPID estimates, and (b)  $34^{\circ}\text{S}$  compared to SAMBA record. Horizontal scale is compressed prior to year 2000.

**Figure 5:** Schematic overview of the ocean features in the Benguela region (from Emeis et al., 2009) Bathymetry of the South East Atlantic (shaded colours) with climatological sea surface temperatures (contour lines in  $^{\circ}\text{C}$ , from Gouretski and Koltermann, 2004). Surface currents are represented by solid lines and subsurface currents by dashed lines. AC Angola Current, ABFZ Angola-Benguela frontal zone, BC Benguela ocean current, BCC Benguela coastal current, PU poleward undercurrent, SEC south equatorial current, SECC south equatorial counter current.

**Figure 6:** Upper-ocean horizontal current (in  $\text{cm s}^{-1}$ ) vertically averaged from 0m to 30m for (a) OSCAR and (b) GLOB16 over the period 2009-2022. Arrows indicate the flow direction, and the shading represents magnitude.

**Figure 7:** Annual mean sea surface temperature ( $^{\circ}\text{C}$ ) for (a) the ESA CCI SST v2.0 and (b) GLOB16 over the period 2009-2022. Contour interval is  $1^{\circ}\text{C}$  for SST below  $17^{\circ}\text{C}$ , and  $0.5^{\circ}\text{C}$  above.

**Figure 8:** The CMCC Data Delivery System home page (<https://dds.cmcc.it>). Version 2 of the dataset is visible in the middle-right box.

**Figure 9:** Example Python script for the download of the data using the DDS API client showing how to perform spatial subsetting.

## 9 References

---

Chassignet, E. P. and Xu, X.: Impact of horizontal resolution ( $1/12^{\circ}$  to  $1/50^{\circ}$ ) on Gulf Stream separation, penetration, and variability, *J. Phys. Oceanogr.*, 47, 1999–2021, doi:[10.1175/JPOD-17-0031.1](https://doi.org/10.1175/JPOD-17-0031.1), 2017.

Chassignet, E. P., Yeager, S. G., Fox-Kemper, B., Bozec, A., Castruccio, F., Danabasoglu, G., Horvat, C., Kim, W. M., Koldunov, N., Li, Y., Lin, P., Liu, H., Sein, D. V., Sidorenko, D., Wang, Q., and Xu, X.: Impact of horizontal resolution on global ocean–sea ice model simulations based on the experimental protocols of the Ocean Model Intercomparison Project phase 2 (OMIP-2), *Geosci. Model Dev.*, 13, 4595–4637, doi:[10.5194/gmd-13-4595-2020](https://doi.org/10.5194/gmd-13-4595-2020), 2020.

Cheng, L. J., K. E. Trenberth, J. Fasullo, T. Boyer, J. Abraham, and J. Zhu: Improved estimates of ocean heat content from 1960 to 2015. *Science Advances*, 3, e1601545, doi:[10.1126/sciadv.1601545](https://doi.org/10.1126/sciadv.1601545), 2017.



ESR; Dohan, K.: Ocean Surface Current Analyses Real-time (OSCAR) Surface Currents - Final 0.25 Degree (Version 2.0). Ver. 2.0. PO.DAAC, CA, USA. doi:[10.5067/OSCAR-25F20](https://doi.org/10.5067/OSCAR-25F20), 2022.

Emeis, K.C., Struck, U., Leipe, T. and Ferdelman T.G.: Variability in upwelling intensity and nutrient regime in the coastal upwelling system offshore Namibia: results from sediment archives. *Int. J. Earth Sci. (Geol. Rundsch.)* 98, 309–326, doi:[10.1007/s00531-007-0236-5](https://doi.org/10.1007/s00531-007-0236-5), 2009.

Good, S., Fiedler, E., Mao, C., Martin, M.J., Maycock, A., Reid, R., Roberts-Jones, J., Searle, T., Waters, J., While, J., Worsfold, M. The Current Configuration of the OSTIA System for Operational Production of Foundation Sea Surface Temperature and Ice Concentration Analyses. *Remote Sens.*, 12, doi:[10.3390/rs12040720](https://doi.org/10.3390/rs12040720), 2020.

Couretski, V., and K. Koltermann: WOCE Global Hydrographic Climatology. *Berichte des BSH 35. Bundesamtes für Seeschifffahrt und Hydrographie, Hamburg, Germany.* ISSN: 0946-6010, 2004.

Griffies, S. M., Danabasoglu, G., Durack, P. J., Adcroft, A. J., Balaji, V., Böning, C. W., Chassignet, E. P., Curchitser, E., Deshayes, J., Drange, H., Fox-Kemper, B., Gleckler, P. J., Gregory, J. M., Haak, H., Hallberg, R. W., Heimbach, P., Hewitt, H. T., Holland, D. M., Ilyina, T., Jungclaus, J. H., Komuro, Y., Krasting, J. P., Large, W. G., Marsland, S. J., Masina, S., McDougall, T. J., Nurser, A. J. G., Orr, J. C., Pirani, A., Qiao, F., Stouffer, R. J., Taylor, K. E., Treguier, A. M., Tsujino, H., Uotila, P., Valdivieso, M., Wang, Q., Winton, M., and Yeager, S. G.: OMIP contribution to CMIP6: experimental and diagnostic protocol for the physical component of the Ocean Model Intercomparison Project, *Geosci. Model Dev.*, 9, 3231–3296, doi:[10.5194/gmd-9-3231-2016](https://doi.org/10.5194/gmd-9-3231-2016), 2016.

Hardman-Mountford N.J., Richardson A.J., Agenbag J.J., Hagen E., Nykjaer L., Shillington F.A., Villacastin C.: Ocean climate of the South East Atlantic observed from satellite data and wind models. *Prog Oceanogr* 59:181–221, doi:[10.1016/j.pocean.2003.10.001](https://doi.org/10.1016/j.pocean.2003.10.001), 2003.

Hutchings, L., van der Lingen, C.D., Shannon, L.J., Crawford, R.J.M., Verheye, H.M.S., Bartholomae, C.H., van der Plas, A.K., Louw, D., Kreiner, A., Ostrowski, M., Fidel, Q., Barlow, R.G., Lamont, T., Coetzee, J., Shillington, F., Veitch, J., Currie, P.M.S. Monteir, J.C.: The Benguela Current: An Ecosystem of Four Components. *Prog. Oceanogr.*, 83, doi:[10.1016/j.pocean.2009.07.046](https://doi.org/10.1016/j.pocean.2009.07.046), 2009.

Iovino D., Fogli P. G. and Masina S.: AtlantECO deliverable D6.1- Dataset of ocean reanalysis and hindmost simulation version 1 (v1.0). Zenodo. doi:[10.5281/zenodo.6405281](https://doi.org/10.5281/zenodo.6405281), 2022.

Iovino, D., Fogli, P. G., and Masina, S.: Evaluation of the CMCC global eddy ocean model for the Ocean Model Intercomparison Project (OMIP2), *EGUsphere* [preprint], doi:[10.5194/egusphere-2023-469](https://doi.org/10.5194/egusphere-2023-469), 2023.

Kuhlbrodt, T., Griesel, A., Montoya, M., Levermann, A., Hofmann, M., and Rahmstorf, S.: On the driving processes of the Atlantic meridional overturning circulation, *Rev. Geophys.*, 45, RG2001, doi:[10.1029/2004RG000166](https://doi.org/10.1029/2004RG000166), 2007.

Manral D, Iovino D, Jaillon O, Masina S, Sarmento H, Iudicone D, Amaral-Zettler L and van Sebille E.: Computing marine plankton connectivity under thermal constraints. *Front. Mar. Sci.* 10:1066050. doi:[10.3389/fmars.2023.1066050](https://doi.org/10.3389/fmars.2023.1066050), 2023.

Meinen, C. S., Speich, S., Piola, A. R., Ansorge, I., Campos, E., Kersalé, M., Terre, T., Chidichimo, M.P., Lamont, T., Sato, O.T., Perez, R.C., Valla, D., van den Berg, M., Le Hénaff, M., Dong, S., Garzoli, S.L.: Meridional overturning circulation transport variability at 34.5°S during 2009–2017: Baroclinic and barotropic flows and the dueling influence of the boundaries. *Geophysical Research Letters*, 45, 4180–4188. <https://doi.org/10.1029/2018GL077408>, 2018.



Moat B.I.; Frajka-Williams E.; Smeed D.; Rayner D.; Johns W.E.; Baringer M.O.; Volkov D.L.; Collins J.: Atlantic meridional overturning circulation observed by the RAPID-MOCHA-WBTS (RAPID-Meridional Overturning Circulation and Heatflux Array-Western Boundary Time Series) array at 26N from 2004 to 2020 (v2020.2). NERC EDS British Oceanographic Data Centre NOC. doi:[10.5285/e91b10af-6f0a-7fa7-e053-6c86abc05a09](https://doi.org/10.5285/e91b10af-6f0a-7fa7-e053-6c86abc05a09), 2022.

Pillar, H. R., P. Heimbach, H. L. Johnson, and D. P. Marshall: Dynamical Attribution of Recent Variability in Atlantic Overturning. *J. Climate*, 29, 3339–3352, doi:[10.1175/JCLI-D-15-0727.1](https://doi.org/10.1175/JCLI-D-15-0727.1), 2016.

Shannon, L.V., 1985. The Benguela Ecosystem, Part 1. Evolution of the Benguela, physical features and processes. *Oceanography and Marine Biology: An Annual Review* 23, 105–182.

Treguier, A. M., de Boyer Montégut, C., Bozec, A., Chassignet, E. P., Fox-Kemper, B., Hogg, A., Iovino, D., Kiss, A. E., LeSommer, J., Li, Y., Lin, P., Lique, C., Liu, H., Serazin, G., Sidorenko, D., Wang, Q., Xu, X., and Yeager, S.: The Mixed Layer Depth in the Ocean Model Intercomparison Project (OMIP): Impact of Resolving Mesoscale Eddies, *Geosci. Model Dev.*, 16,3849–3872, doi:[10.5194/gmd-16-3849-2023](https://doi.org/10.5194/gmd-16-3849-2023), 2023.

Tsujino, H., Urakawa, S., Nakano, H., Small, R. J., Kim, W. M., Yeager, S. G., Danabasoglu, G., Suzuki, T., Bamber, J. L., Bentsen, M., Böning, C. W., Bozec, A., Chassignet, E. P., Curchitser, E., Boeira Dias, F., Durack, P. J., Griffies, S. M., Harada, Y., Ilicak, M., Josey, S. A., Kobayashi, C., Kobayashi, S., Komuro, Y., Large, W. G., Le Sommer, J., Marsland, S. J., Masina, S., Scheinert, M., Tomita, H., Valdivieso, M., and Yamazaki, D.: JRA-55 based surface dataset for driving ocean–sea-ice models (JRA55-do), *Ocean Model.*, 130, 79–139, doi:[10.1016/j.ocemod.2018.07.002](https://doi.org/10.1016/j.ocemod.2018.07.002), 2018.

Tsujino H., Shogo Urakawa L., Nakano H., Small R.J., Kim W.M., Yeager S.G., Danabasoglu G., Suzuki T., Bamber J.L., Bentsen M., Böning C., Bozec A., Chassignet E., Curchitser E., Boeira Dias F., Durack P.J., Griffies S.M., Harada Y., Ilicak M., Josey S.A., Kobayashi C., Kobayashi S., Komuro Y., Large W.G., Le Sommer J., Marsland S.J., Masina S., Scheinert M., Tomita H., Valdivieso M., Yamazaki D.: User manual of JRA-55 based surface dataset for driving ocean–sea-ice models (JRA55-do), URL:[https://climate.mri-jma.go.jp/pub/ocean/JRA55-do/docs/v1\\_5-manual/User\\_manual\\_jra55\\_do\\_v1\\_5.pdf](https://climate.mri-jma.go.jp/pub/ocean/JRA55-do/docs/v1_5-manual/User_manual_jra55_do_v1_5.pdf), June 9, 2021.

Wang, Q., Shu, Q., Bozec, A., Chassignet, E. P., Fogli, P. G., Fox-Kemper, B., Hogg, A. McC., Iovino, D., Kiss, A. E., Koldunov, N., Le Sommer, J., Li, Y., Lin, P., Liu, H., Polyakov, I., Scholz, P., Sidorenko, D., Wang, S., and Xu, X.: Impact of high resolution on Arctic Ocean simulations in Ocean Model Intercomparison Project phase 2 (OMIP-2), *Geosci. Model Dev. Discuss.* [preprint], doi:[10.5194/gmd-2023-123](https://doi.org/10.5194/gmd-2023-123), under review, 2023.